ISSN 1674-1056
http://cpb.iphy.ac.cn
http://iopscience.iop.org/cpb
中国物理 B
Chinese Physics
中国物理
Chinese Physics B

Pancharatnam-Berry metasurface for terahertz wave radar cross section reduction

Shao-He Li(李绍和), Jiu-Sheng Li(李九生)
Citation: Chin. Phys. B . 2019, 28(9): 094210 . **doi:** 10.1088/1674-1056/28/9/094210
Journal homepage: http://cpb.iphy.ac.cn; http://iopscience.iop.org/cpb

What follows is a list of articles you may be interested in

Light-scattering model for aerosol particles with irregular shapes and inhomogeneous compositions using a parallelized pseudo-spectral time-domain technique

Shuai Hu(胡帅), Taichang Gao(高太长), Hao Li(李浩), Lei Liu(刘磊), Ming Chen(陈鸣), Bo Yang(杨波)
Chin. Phys. B . 2018, 27(5): 054215 . **doi:** 10.1088/1674-1056/27/5/054215

Theoretical studies on particle shape classification based on simultaneous small forward angle light scattering and aerodynamic sizing

Jin-Bi Zhang(张金碧), Lei Ding(丁蕾), Ying-Ping Wang(王颖萍), Li Zhang(张莉), Jin-Lei Wu(吴金雷), Hai-Yang Zheng(郑海洋), Li Fang(方黎)
Chin. Phys. B . 2016, 25(3): 034201 . **doi:** 10.1088/1674-1056/25/3/034201

Electromagnetic scattering of the carbon nanotubes excited by an electric line source

Wang Yue, Wu Qun, Wu Yu-Ming, He Xun-Jun, Li Le-Wei
Chin. Phys. B . 2012, 21(1): 014212 . **doi:** 10.1088/1674-1056/21/1/014212

Pancharatnam–Berry metasurface for terahertz wave radar cross section reduction*

Shao-He Li(李绍和) and Jiu-Sheng Li(李九生)†

Center for THz Research, China Jiliang University, Hangzhou 310018, *China*

(Received 24 March 2019; revised manuscript received 9 June 2019; published online 7 August 2019)

The digital coding metasurfaces need several kinds of meta-particle structures to obtain corresponding electromagnetic wave responses and require time-consuming optimization. In this paper, we present train-symbol-shaped meta-particles with various orientations utilizing Pancharatnam–Berry (PB) phase to achieve 1-, 2-, and 3-bit digital coding metasurfaces. Terahertz wave scattering patterns of the coding metasurfaces with regular and random sequences are given and discussed. They have strongly suppressed backward scattering with approximately −13.5 dB radar cross section (RCS) reduction in a wide band range from 0.85 THz to 1.6 THz. The proposed digital coding metasurfaces provide a simple way and new opportunities for manipulating terahertz wave scattering with polarization independence.

Keywords: terahertz metasurface, terahertz optics, terahertz polarization

PACS: 42.68.Mj **DOI:** 10.1088/1674-1056/ab33f5

1. Introduction

Metasurface is an ultra-thin two-dimensional metamaterial composed of particles with different phases, it not only overcomes the shortcomings of the metamaterial in controlling electromagnetic wave,[1,2] such as bulky thickness and great loss, but also improves the ability of manipulating the electromagnetic wave significantly. The metal-particles of the metasurface provide phase discontinuities, thus electromagnetic waves can be manipulated at will. By changing the phase metasurface distribution and carefully designing the metasurface parameters, many applications can be achieved, including polarization conversion,[3–5] invisibility skin cloak,[6,7] quarter-wave plate,[8] focus,[9] and hologram.[10,11] More recently, coding metasurfaces have been studied widely and provided a new way to manipulate the terahertz wave.[12–20] However, most of these devices require several kinds of different structural and different sizes meta-particle unit cells.

In this work, we utilize the train-symbol-shaped meta-particles having a Pancharatnam–Berry (PB) phase as coding elements, which have a co-polarization reflection characteristic under circularly polarized wave incidence. The PB phase is only related to the rotation angle and is independent of the geometry structure. The PB phase meta-particles can be obtained by a rotation of the metal pattern around the z-axis with steps of 22.5° from 0° to 157.5°. The unit cells satisfy the phase requirement and phase coverage of 360°. To generate these PB coding metasurfaces, we consider a general metasurface with an $N\times N$ array of coding elements and each element consists of a 5×5 array of unit cells. Based on the PB phase meta-particles with various orientations, we design the coding elements to achieve 1-, 2-, and 3-bit coding metasurfaces. Compared with other coding metasurfaces, the PB phase coding metasurfaces can manipulate the terahertz wave by coding sequences without changing the meta-particle structure under normal incidence of the left circularly polarized plane (LCP), right circularly polarized plane (RCP), and linearly polarized (LP) waves. Both theoretical analysis and numerical simulation indicate that the proposed PB phase coding metasurfaces have more flexibility in manipulating the terahertz wave and radar cross section (RCS) reduction in a wide frequency band.

2. Theoretical analysis and simulation

2.1. Theory of RCS reduction

For an ordinary metal plate, when electromagnetic waves are vertically irradiated to the surface, an induced current is excited on the surface, which causes backward scattering. Due to in-phase of the induced currents on the surface, it will superimpose in the backward direction to produce a large scattering peak, and the backward radar cross section is very large. Thus, we use multi-bit coding metasurfaces to reduce RCS. The multi-bit coding metasurfaces consist of eight unit cells with a phase difference of 45°. The scattering field is generated by different unit cells and then the RCS can be reduced effectively. However, the coding metasurfaces are not consumable structures, and the energy of the incident electromagnetic wave can not be absorbed by the coding metasurfaces. We can find that the incident electromagnetic wave energy is scattered to different directions. By optimizing the spatial distribution of the meta-particle unit cell, the backward scattering field forms as many beams as possible. According to the law of energy conservation, the RCS can be reduced effectively.

*Project supported by the National Natural Science Foundation of China (Grant Nos. 61871355 and 61831012).

†Corresponding author. E-mail: jshli@126.com

© 2019 Chinese Physical Society and IOP Publishing Ltd

2.2. PB meta-particle design

For a reflection meta-particle under the Cartesian coordinate system, as shown in Fig. 1(a), the reflection matrix after a rotation angle β can be given by

$$\boldsymbol{R} = \begin{bmatrix} \cos\beta & -\sin\beta \\ \sin\beta & \cos\beta \end{bmatrix}^{-1} \begin{bmatrix} r_{xx} & r_{xy} \\ r_{yx} & r_{yy} \end{bmatrix} \begin{bmatrix} \cos\beta & -\sin\beta \\ \sin\beta & \cos\beta \end{bmatrix}, \quad (1)$$

where subscripts x and y denote the polarization of the incidence terahertz wave. The reflection matrix under the circularly polarized (CP) wave can be calculated by

$$\boldsymbol{R}_{\mathrm{LR}} = \frac{1}{2} \begin{bmatrix} 1 & -\mathrm{j} \\ 1 & \mathrm{j} \end{bmatrix} \boldsymbol{R} \begin{bmatrix} 1 & -\mathrm{j} \\ 1 & \mathrm{j} \end{bmatrix}^{-1}. \quad (2)$$

By substituting Eq. (1) into Eq. (2), we derive the following reflection matrix:

$$\begin{cases} r_{\mathrm{LL}} = \frac{1}{2}\left[(r_{xx} - r_{yy}) - \mathrm{j}\,(r_{xy} + r_{yx})\right] \mathrm{e}^{-\mathrm{j}2\beta}, \\ r_{\mathrm{RR}} = \frac{1}{2}\left[(r_{xx} - r_{yy}) + \mathrm{j}\,(r_{xy} + r_{yx})\right] \mathrm{e}^{\mathrm{j}2\beta}, \\ r_{\mathrm{LR}} = \frac{1}{2}\left[(r_{xx} + r_{yy}) + \mathrm{j}\,(r_{xy} - r_{yx})\right], \\ r_{\mathrm{RL}} = \frac{1}{2}\left[(r_{xx} + r_{yy}) - \mathrm{j}\,(r_{xy} - r_{yx})\right]. \end{cases} \quad (3)$$

When $|r_{xy}| \approx |r_{yx}| \approx 1$, $r_{xx} \approx r_{yy} \approx 0$. In order to broaden the operating bandwidth of the PB particle, the phase profile of the designed PB particle has a similar slope at different frequencies, and it can be written as

$$\frac{\partial\varphi(L,R)}{\partial f_1} \approx \frac{\partial\varphi(L,R)}{\partial f_i} \approx \frac{\partial\varphi(L,R)}{\partial f_2}, \quad (4)$$

where f_1 and f_2 are the lower and upper frequencies of the operating band, respectively, f_i indicates an arbitrary frequency within the operating band, and $\varphi(L,R)$ is the reflection phase under LCP/RCP wave illumination.

We know that the scattering wave can be controlled flexibly by specific pre-designed coding sequences formed by several particles with different phase distributions. Generally, an N-bit coding metasurface requires 2^N different meta-particles with optimized geometries to achieve diverse phase shifts for the incident terahertz wave. Specifically, the 1-bit coding metasurface needs two different meta-particles with 180° phase difference. Similarly, the 2-bit coding metasurfaces need four different meta-particles with 90° phase difference. The 3-bit coding metasurfaces need eight different meta-particles with reflection phases of 0°, ±45°, ±90°, ±135°, ±180°, ±225°, ±270°, and ±315°, which correspond to the digital bits of '000', '001', '010', '011', '100', '101', '110', and '111', respectively. A $\pm 2\beta$ reflection phase shift of the PB meta-particle can be realized with a distinct rotation angle β of the top metallic pattern, where "+" and "−" represent the LCP and RCP waves, respectively. The eight meta-particles can be obtained by rotating different angles of the top metallic pattern from 0° to 157.5° with steps of 22.5°. We firstly design a PB coding metasurface based on 50×50 super particles for terahertz beams manipulation. Each super particle consists of 5×5 basic unit cells. Figure 1 shows a meta-particle unit cell, which is composed of a train-symbol-shaped metallic pattern, an intermediate dielectric layer with permittivity $\varepsilon = 3.0$ and loss tangent $\tan\delta = 0.03$, and a metallic ground plate. The metallic pattern and the metallic ground plate are made of copper with a conductivity of 5.8×10^7 S/m and a thickness of 0.2 μm. The period of the unit cell is $P = 75$ μm, and the optimized geometrical parameters marked in the graph are listed as $h = 30$ μm, $L_1 = 20$ μm, $L_2 = 20$ μm, $w = 10$ μm, and $R = 30$ μm.

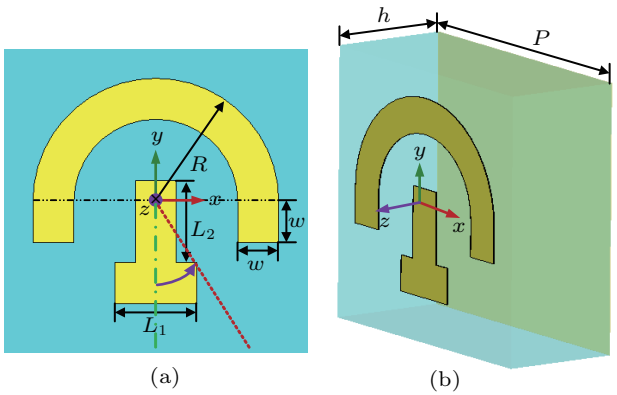


Fig. 1. Illustration of the meta-particle geometries. (a) Top view, (b) three-dimensional view of meta-particle.

The co-polarization (black curve) and cross-polarization (red curve) reflection magnitudes of the PB particle from 0.6 THz to 2 THz under normal incidence of the LCP and RCP waves are calculated by using the commercial software CST, as shown in Fig. 2(a). The cross-polarization reflection magnitude becomes larger than 0.9 (marked with a dotted line) in the frequency from 0.85 THz to 1.6 THz (see the blue area in the picture). On the contrary, the maximum reflection magnitude of co-polarization is lower than 0.2 in the frequency from 0.85 THz to 1.6 THz. Due to the multiple resonant modes, the meta-particle has three different resonant frequencies of 0.88 THz, 1.23 THz, and 1.57 THz respectively. Figure 2(b) shows the characteristics of the PB particle under normal incidence of the x-polarized and y-polarized waves. From the figure, one can see that the reflection amplitudes under normal incidence of the x-polarized and y-polarized waves are larger than 0.85 (marked with a pink dotted line) in the frequency from 0.8 THz to 1.6 THz (see the blue area). The reflected phases under normal incidence of the x-polarized and y-polarized waves reach π (marked with a purple dotted line) in the frequency from 0.8 THz to 1.6 THz.

Figures 3(a) and 3(b) depict the reflection magnitude and reflection phase for cross-polarization with different rotation angle β of the top metallic pattern under LCP or RCP wave normal incidence. The reflection magnitude for cross-polarization of eight meta-particles reaches about 0.9 (marked with a red dotted line) in a wide band (from 0.85 THz to

1.6 THz). Most importantly, one can see that the phase response is parallel as expected within the frequency interval for different rotation angles, where the phase variation is twice of the rotation angle (see the blue area). When the phase increases with 45° steps in the whole frequency from 0.85 THz to 1.6 THz, the reflection magnitude and reflection phase shift of the basic particles are insensitive to the incident angle. Thus, the meta-particle satisfies the requirements of the reflection coefficient matrix and generates the phase shift under LCP or RCP wave by rotating the train-sign-shaped structure. The perfect phase as well as the high cross-polarized reflection efficiency makes the meta-particle for reflective coding metasurface to realize in a wide working bandwidth. Figure 3(c) illustrates the particles of the 1-bit, 2-bit, and 3-bit coding metasurfaces and their corresponding PB phases. One sees that the rotation angle β gradually increases from 0° to 180° with a fixed step. For the 1-bit, 2-bit, or 3-bit coding metasurface, the rotation angle steps of the meta-particles are set as 90°, 45°, or 22.5°, respectively. Figure 3(d) gives the particles of the 1-bit, 2-bit, and 3-bit coding metasurfaces and the relationship between the particle and rotation angle β. For simplicity, we define the numbers 0–7 as '000', '001', '010', '011', '100', '101', '110', and '111', respectively.

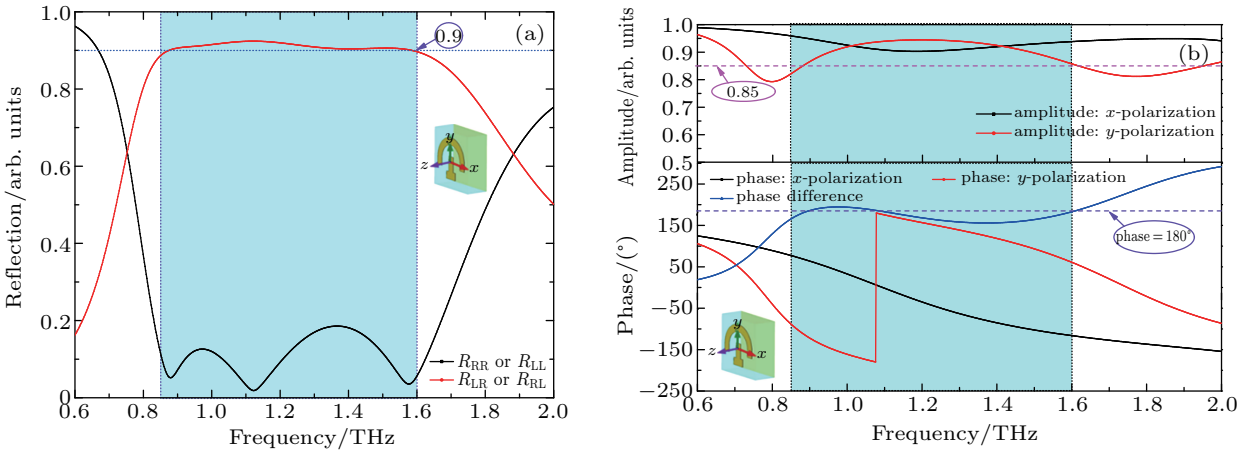
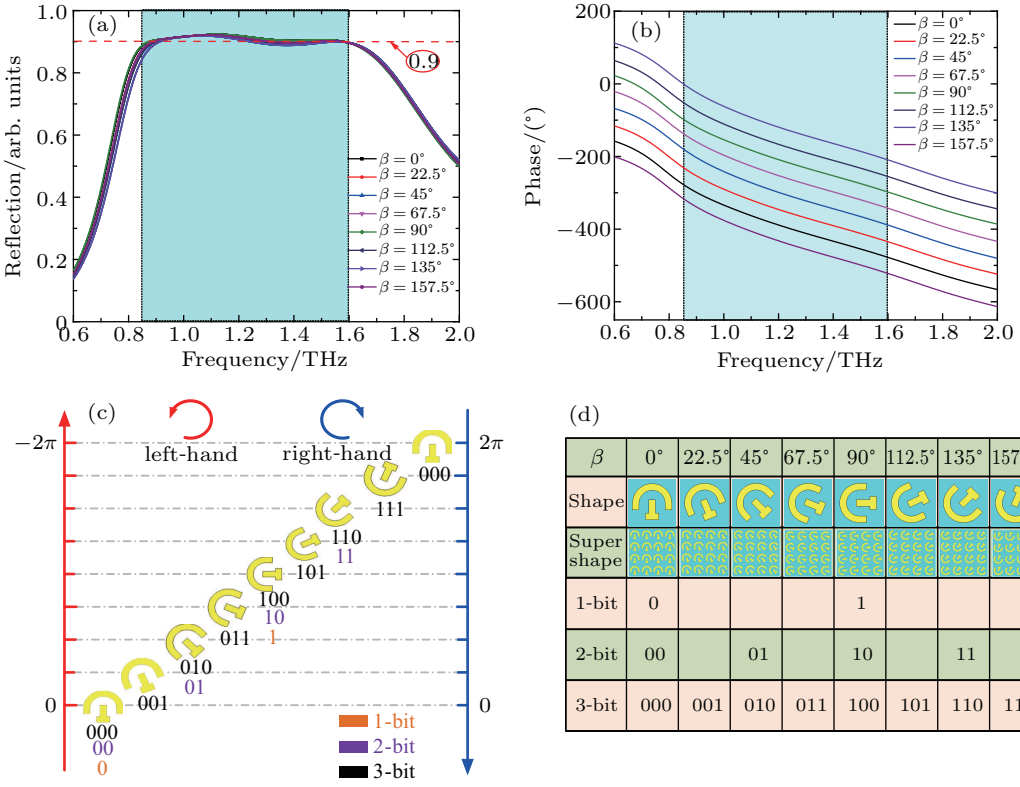


Fig. 2. Characteristics of the basic PB unit cell. (a) Reflection magnitude of the basic unit cell under normal incidence of the LCP or RCP wave. Here, R_{RR} (R_{LL}) and R_{LR} (R_{RL}) represent the reflection magnitudes of co-polarization and cross-polarization under vertical radiation of LCP (RCP) wave, respectively. (b) Reflection amplitude and reflection phase under normal incidence of the x-polarized and y-polarized waves.



(d)

β	0°	22.5°	45°	67.5°	90°	112.5°	135°	157.5°
Shape								
Super shape								
1-bit	0				1			
2-bit	00		01		10		11	
3-bit	000	001	010	011	100	101	110	111

Fig. 3. Spectrum information of the PB metasurface particles under normal incidence of LCP and RCP waves. (a) The reflection magnitude for cross-polarization with different rotation angle β. (b) The reflection phase for cross-polarization with different rotation angle β. (c) The 1-bit, 2-bit, and 3-bit coding metasurface unit cells and their corresponding PB phases.(d) The basic parameters of eight coding elements for the 1-bit, 2-bit, and 3-bit coding metasurfaces.

2.3. Coding metasurface design

The coding metasurface consists of $N \times N$ super particles, which is illuminated by a normal incident terahertz wave. The far-field radiation pattern $F(\theta,\varphi)$ is expressed as

$$F(\theta,\varphi) = \sum_{m=1}^{N}\sum_{n=1}^{N} \exp\left\{-\mathrm{i}\left[\left(\frac{2\pi}{\lambda}L(m-1/2)\sin\theta\cos\varphi + \frac{2\pi}{\lambda}L(n-1/2)\sin\theta\sin\varphi\right) + \varphi(m,n)\right]\right\}, \quad (5)$$

where φ and θ represent the azimuth and elevation angles, respectively. $\varphi(m,n)$ is the reflection phase of the super particle, and $\varphi(m,n)=0$ and $\varphi(m,n)=\pi$ denote "0" and "1" elements, respectively. L is the side length of the super-particle, and λ is the free-space wavelength of the working frequency. As the elevation angle θ and the azimuth angle φ satisfy the following relations: $\varphi = \pm\arctan(\Gamma_x/\Gamma_y)$, $\varphi = \pi \pm \arctan(\Gamma_x/\Gamma_y)$, and $\theta = \arcsin\left(\lambda\sqrt{1/\Gamma_x^2+1/\Gamma_y^2}\right)$, the function $|F(\theta,\varphi)|$ will achieve the maximum value, where Γ_x and Γ_y are the physical periodic lengths of the phase gradient coding sequence along the x and y directions, respectively. In this section, we design multiple PB coding metasurfaces consisting of 40×40 super-particles. Each super-particle consists of 5×5 basic unit cells, and the size of the super-particle is $D = 5\times75 = 275$ μm.

The scattering field pattern of the PB phase coding metasurface can be achieved by the pre-designed coding sequence. Here, we design 3-bit regular coding metasurfaces (8×8 super particles) generated by the pre-designed coding sequence to verify the scattering field pattern. Figure 4 shows the three-dimensional (3D) and two-dimensional (2D) far-field scattering patterns under normal incidence of the LCP, RCP, and LP waves at 1.2 THz by coding metasurface 1, which is generated with the pre-designed coding sequence of 0, 1, 2, 3, 4, 5, 6, 7 along x-direction while invariant along y-direction. Due to the phase distribution of the coding metasurface 1 having exactly the opposite constant gradient between the LCP and RCP waves, a main lobe appears on either side of the z axis at the elevation angle of 6° under the illumination of the LCP or RCP incident wave. There are two beams of mirror side-lobe with the elevation angle $\theta_1 = 6°$ and azimuth angle $\varphi = 0°$ or 180° under the illumination of the LP wave, as displayed in Fig. 4(b). The elevation angle is given by $\theta_1 = \arcsin(\lambda/\Gamma_1)$, where λ is the wavelength in free space at 1.2 THz, $\Gamma_1 = 8\times275$ μm is the physical period length of the coding metasurface 1. Meanwhile, we also design coding metasurface 2 with the pre-designed coding sequence of 0, 1, 2, 3, 4, 5, 6, 7 along y-direction while invariant along x-direction. As shown in Fig. 4(b), the normal incident LP wave is reflected into two symmetrical orientations. The azimuth angles of the two reflected beams change from $\varphi = 0°$ or 180° to $\varphi = 90°$ or 270°, while the elevation angle is still $\theta_2 = \theta_1 = 6°$. The simulated 2D far-field radiation patterns are in good agreement with the theoretical predicted results.

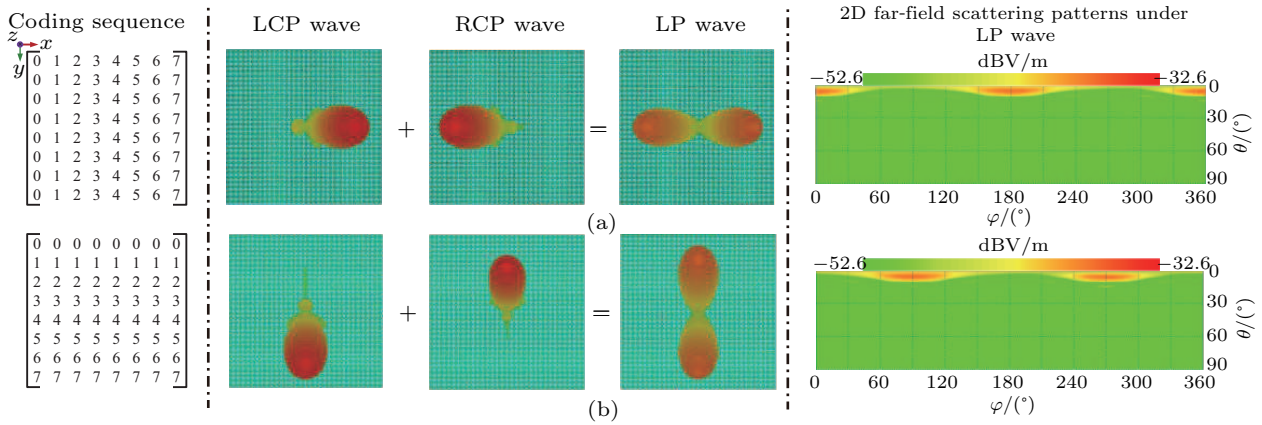


Fig. 4. The 3D and 2D far-field scattering patterns of coding metasurfaces 1 and 2 at 1.2 THz. (a) Coding metasurface 1 with pre-designed coding sequence of 0, 1, 2, 3, 4, 5, 6, 7 along x-direction while invariant along y-direction. (b) Coding metasurface 2 with pre-designed coding sequence of 0, 1, 2, 3, 4, 5, 6, 7 along y-direction while invariant along x-direction.

We design four kinds of coding metasurfaces to analyze the far-field scattering patterns of these coding metasurfaces, as illustrated in Figs. 5 and 6. As shown in Figs. 5(a) and 5(b), the coding metasurfaces are arranged with the pre-designed coding sequences of 0, 1, 2, 3, 4, 5, 6, 7/4, 5, 6, 7, 0, 1, 2, 3 along x-direction and y-direction, which are denoted as coding metasurfaces 3 and 4, respectively. Figure 5(a) depicts the coding metasurface 3 with a constant phase gradient along x-direction and π phase difference along y-direction. From the figure, it can be noted that the normal incident LCP terahertz wave is reflected into two beams with directions ($\theta_3 = 24.6°$, $\varphi = 76°$) and ($\theta_3 = 24.6°$, $\varphi = 284°$). For RCP terahertz wave normal incidence, the elevation angles of the reflected two symmetrical orientations become ($\theta_3 = 24.6°$, $\varphi = 104°$) and ($\theta_3 = 24.6°$, $\varphi = 256°$). One can also find that the normal incident LP wave is reflected into four symmetrical directions with the elevation angles of ($\theta_3 = 24.6°$, $\varphi = 76°$), ($\theta_3 = 24.6°$, $\varphi = 104°$), ($\theta_3 = 24.6°$, $\varphi = 284°$), and ($\theta_3 = 24.6°$,

$\varphi = 256°$), where $\theta_3 = \arcsin(\lambda/\Gamma_3)$, λ is the wavelength in free space at 1.2 THz, $\Gamma_3 = 4 \times 275$ μm is the physical period length of the coding metasurface 3. For coding metasurface 4, as shown in Fig. 5(b), the normal incident LP wave is reflected into four symmetrical directions with the elevation angles of ($\theta_4 = \theta_3 = 24.6°$, $\varphi = 14°$), ($\theta_4 = \theta_3 = 24.6°$, $\varphi = 166°$), ($\theta_4 = \theta_3 = 24.6°$, $\varphi = 194°$), and ($\theta_4 = \theta_3 = 24.6°$, $\varphi = 314°$). While the two symmetrical directions have the elevation angles of ($\theta_4 = \theta_3 = 24.6°$, $\varphi = 194°$) and ($\theta_4 = \theta_3 = 24.6°$, $\varphi = 314°$) for the LCP wave and ($\theta_4 = \theta_3 = 24.6°$, $\varphi = 14°$) and ($\theta_4 = \theta_3 = 24.6°$, $\varphi = 166°$) for the RCP wave. From Fig. 5, the simulation results of these two coding metasurfaces in the 2D far-field radiation patterns are in good agreement with the theoretical predicted results.

Similarly, as shown in Fig. 6(a), for the coding metasurface 5 with the coding sequence of 0, 1, 2, 3, 4, 5, 6, 7/0, 1, 2, 3, 4, 5, 6, 7/4, 5, 6, 7, 0, 1, 2, 3 along x-direction, the reflected waves with the elevation angles of ($\theta_1 = 6°$, $\varphi = 0°$), ($\theta_5 = 16.1°$, $\varphi = 69.4°$), and ($\theta_5 = 16.1°$, $\varphi = 290.6°$) or ($\theta_1 = 6°$, $\varphi = 180°$), ($\theta_5 = 16.1°$, $\varphi = 110.6°$), and ($\theta_5 = 16.1°$, $\varphi = 249.4°$) appear on both sides of the z axis under the normal incident of the LCP and RCP waves, respectively. Thereby, the normal incident LP wave is reflected into six symmetrical directions with ($\theta_1 = 6°$, $\varphi = 0°$), ($\theta_5 = 16.1°$, $\varphi = 69.4°$), ($\theta_5 = 16.1°$, $\varphi = 290.6°$), ($\theta_1 = 6°$, $\varphi = 180°$), ($\theta_5 = 16.1°$, $\varphi = 110.6°$), and ($\theta_5 = 16.1°$, $\varphi = 249.4°$). Figure 6(b) shows the 3D far-field scattering patterns of coding metasurface 6 with the coding sequence of 0, 1, 2, 3, 4, 5, 6, 7/0, 1, 2, 3, 4, 5, 6, 7/4, 5, 6, 7, 0, 1, 2, 3 along y-direction. The normal incident LCP terahertz wave is reflected into 3-bundle side-lobe with the elevation angles of ($\theta_1 = 6°$, $\varphi = 90°$), ($\theta_6 = \theta_5 = 16.1°$, $\varphi = 20.6°$), and ($\theta_6 = \theta_5 = 16.1°$, $\varphi = 159.4°$). Similarly, the RCP terahertz wave normal incidence is reflected into 3-bundle side-lobe with the elevation angles of ($\theta_1 = 6°$, $\varphi = 270°$), ($\theta_6 = \theta_5 = 16.1°$, $\varphi = 200.6°$), and ($\theta_6 = \theta_5 = 16.1°$, $\varphi = 339.4°$). Therefore, the normal incidence LP wave is reflected into six symmetrical directions with the angles of ($\theta_1 = 6°$, $\varphi = 90°$), ($\theta_6 = \theta_5 = 16.1°$, $\varphi = 20.6°$), ($\theta_6 = \theta_5 = 16.1°$, $\varphi = 159.4°$), ($\theta_1 = 6°$, $\varphi = 270°$), ($\theta_6 = \theta_5 = 16.1°$, $\varphi = 200.6°$), and ($\theta_6 = \theta_5 = 16.1°$, $\varphi = 339.4°$), as shown in Fig. 6.

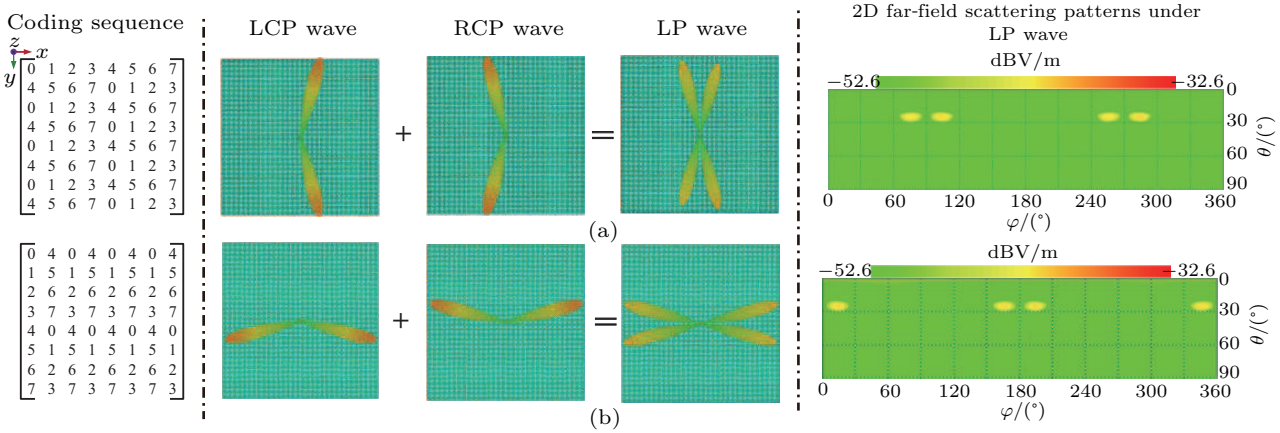


Fig. 5. The 3D and 2D far-field scattering patterns of coding metasurfaces 3 and 4 at 1.2 THz.(a) Coding metasurface 3 with pre-designed coding sequence of 0, 1, 2, 3, 4, 5, 6, 7/4, 5, 6, 7, 0, 1, 2, 3 along x-direction.(b) Coding metasurface 4 with pre-designed coding sequence of 0, 1, 2, 3, 4, 5, 6, 7/4, 5, 6, 7, 0, 1, 2, 3 along y-direction.

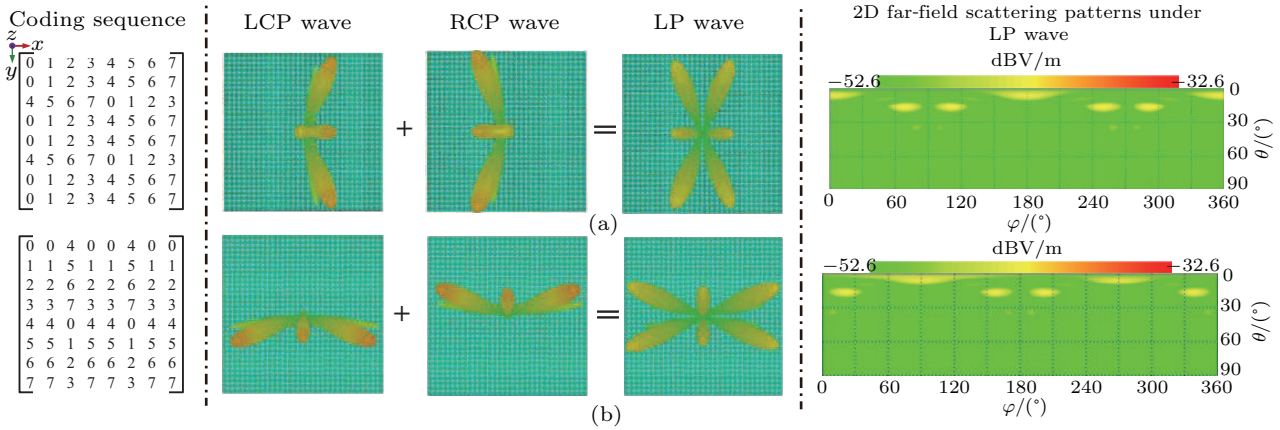


Fig. 6. The 3D and 2D far-field scattering patterns of coding metasurfaces 5 and 6 at 1.2 THz. (a) Coding metasurface 5 with pre-designed coding sequence of 0, 1, 2, 3, 4, 5, 6, 7/0, 1, 2, 3, 4, 5, 6, 7/4, 5, 6, 7, 0, 1, 2, 3 along x-direction. (b) Coding metasurface 6 with pre-designed coding sequence of 0, 1, 2, 3, 4, 5, 6, 7/0, 1, 2, 3, 4, 5, 6, 7/4, 5, 6, 7, 0, 1, 2, 3 along y-direction.

2.4. Bi-static RCS reduction

To verify the suppressing backward scattering characteristics, we design 1-bit, 2-bit, and 3-bit coding metasurfaces with random coding sequences and calculate the bi-static radar cross section under LCP-, RCP-, and LP-wave normal incidence. Each random coding metasurface consists of 8×8 super particles with coding sequence which is generated by MATLAB. Due to the phase of these coding metasurfaces is randomly distributed, it redirects the incident terahertz wave to numerous directions and generates a lot of side-lobes with smaller energy which greatly suppresses backward scattering. The radar cross sections of the bare metallic plate and 1-bit, 2-bit, and 3-bit random coding metasurfaces with the same size are shown in Figs. 7(a)–7(c) under LCP, RCP, and LP wave normal incidence within the frequency range from 0.85 THz to 1.6 THz. The maximum RCS reductions of the 1-bit, 2-bit, and 3-bit random coding metasurfaces are −24.1 dB, −20.7 dB, and −22.8 dB, respectively. As the RCS under the LP wave normal incidence is almost identical compared with those of the LCP and RCP waves, it has no influence on the RCS reduction for the 1-bit, 2-bit, and 3-bit random coding metasurfaces. This proves that the coding metasurfaces have polarization insensitive property in RCS reduction.

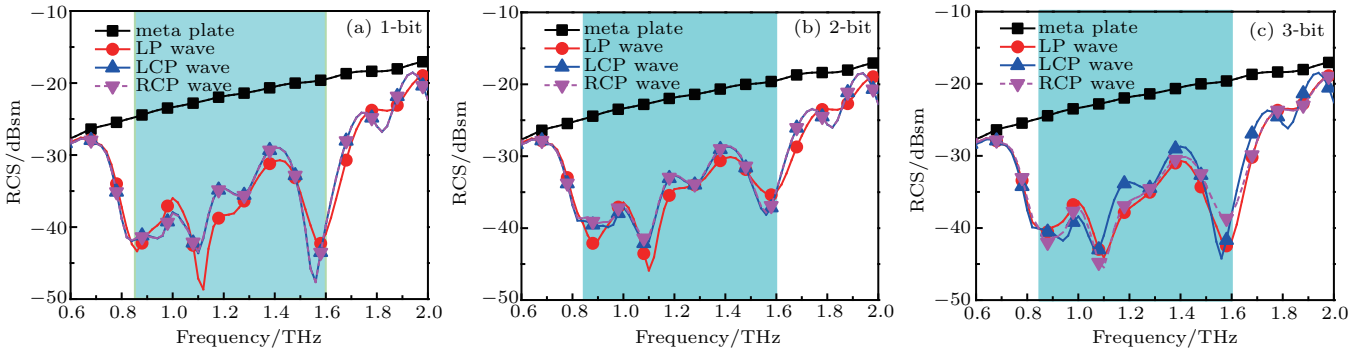


Fig. 7. RCS for (a) 1-bit, (b) 2-bit, and (c) 3-bit random coding metasurfaces under normal incidence of the RCP, LCP, and LP waves.

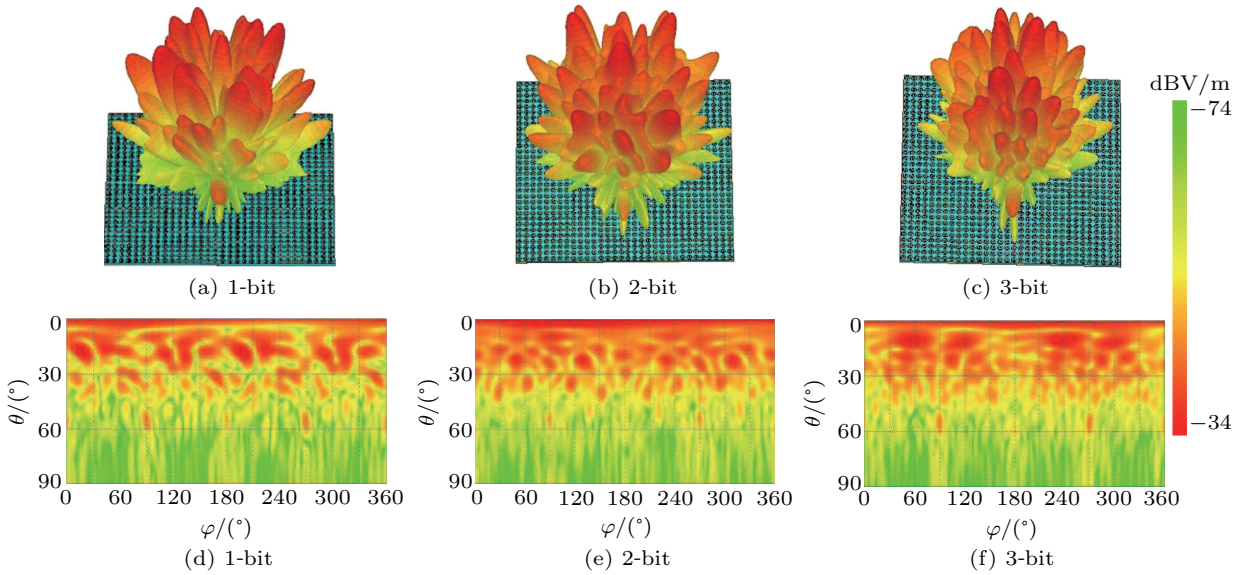


Fig. 8. The (a)–(c) 3D and (d)–(f) 2D far-field scattering patterns of 1-bit, 2-bit, 3-bit random coding metasurfaces under LP wave normal incidence at 1.2 THz.

In addition, we simulate the 3D and 2D far-field radiation patterns of the 1-bit, 2-bit, and 3-bit random coding metasurfaces in a vertical plane at 1.2 THz under the normal illumination of the LP wave, as depicted in Fig. 8. Form Figs. 8(a)–8(c), one sees that the incident terahertz LP wave is reflected into numerous directions by the PB coding metasurfaces. Figures 8(d)–8(e) show the energy scattering patterns in numerous directions. The bi-static RCS distributions of the 1-bit, 2-bit, and 3-bit random PB coding metasurfaces and the same size bare metal plate have been simulated under the LP wave vertical incidence at 1.2 THz, as depicted in Fig. 9. It is obviously that the RCS reduction of the random PB coding metasurfaces is larger than 13.5 dB. This phenomenon can be explained by the law of energy conservation that the scattered energy of each reflected wave beam is low because the terahertz wave is reflected into numerous directions. Figure 10 depicts the near-

field energy distribution of the random coding PB metasurfaces at 1.2 THz in vertical-plane patterns, by which the RCS reduction is further verified. Here, we provide the calculation of the RCS of a coding metasurface for 45° oblique incidence angle, as shown in Fig. 11. Compared with the normally incident radiation condition (see Fig. 7), the bi-static RCS distributions of the 1-bit, 2-bit, and 3-bit random PB coding metasurfaces decrease slightly in the frequency from 0.85 THz to 1.6 THz. The PB coding metasurface significantly reduces RCS for incidence angles between 0° and 45° in a spectral working range from 0.85 THz to 1.6 THz.

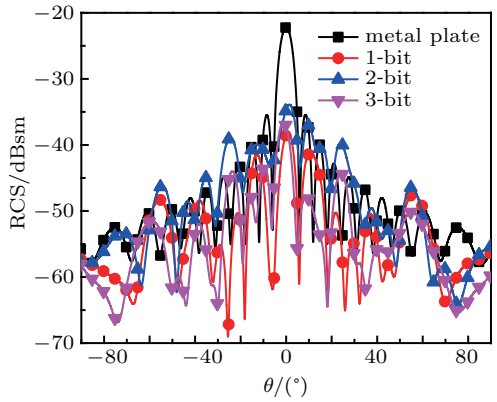


Fig. 9. RCS distribution for the coding metasurfaces and bare metal plate under normal incidence of the LP wave at 1.2 THz.

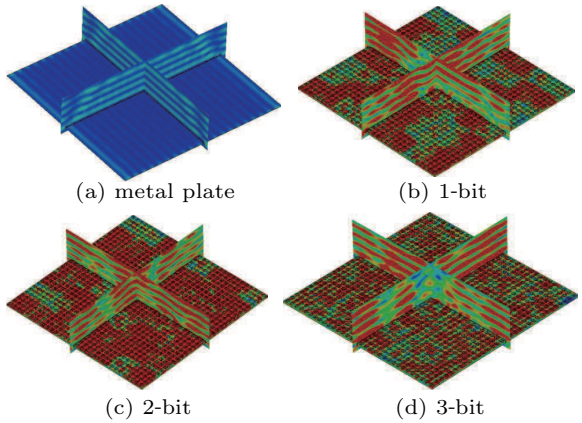


Fig. 10. Near-electric-field energy distributions of (a) bare metal plate, (b) 1-bit, (c) 2-bit, and (d) 3-bit coding metasurfaces in vertical plane under normal incidence of the LP wave at 1.2 THz.

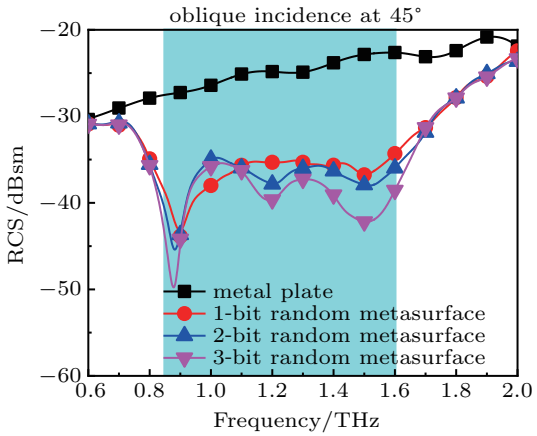


Fig. 11. RCS distribution for 1-bit, 2-bit, 3-bit random coding metasurfaces under oblique incident at 45°.

3. Conclusion

We theoretically analyzed and demonstrated the RCS reduction properties of the PB metasurface for 0°–45° obliquely incident radiation in a spectral working range from 0.85 THz to 1.6 THz. The designed 1-bit, 2-bit, and 3-bit PB coding metasurfaces generated by random coding sequences can produce scattering waves in all directions and suppress backward scattering strongly. The designed PB coding metasurface has 13.5 dB RCS reduction and is polarization-insensitive. It provides the ability of the wide-band RCS reduction and a flexible way to manipulate the terahertz wave.

Acknowledgment

The authors thank Prof. J. Q. Yao for his helpful discussion.

References

[1] Zhang K, Wu Q, Fu J H, Meng F Y and Li L W 2012 *IEEE Trans. Magn.* **48** 4289
[2] Shi H Y, Zhang A X, Zheng S, Li J X and Jiang Y S 2014 *Appl. Phys. Lett.* **104** 034102
[3] Grady N K, Heyes J E, Chowdhury D R, Zeng Y, Reiten M T, Azad A K, Taylor A J, Dalvit D A R and Chen H T 2013 *Science* **340** 1304
[4] Li Y F, Zhang J Q, Qu S B, Wang J F, Zheng L, Pang Y Q, Xu Z and Zhang A X 2015 *J. Appl. Phys.* **117** 044501
[5] Huang X J, Chen J and Yang H L 2017 *J. Appl. Phys.* **122** 043102
[6] Estakhri N M and Alu A 2014 *IEEE Antennas Wireless Propag. Lett.* **13** 1775
[7] Ni X, Wong Z J, Mrejen M, Wang Y and Zhang X 2015 *Science* **349** 1310
[8] Yu N F, Aieta F, Genevet P, Kats M A, Gaburro Z and Capasso F 2012 *Nano Lett.* **12** 6328
[9] Li X, Xiao S Y, Cai B G, He Q, Cui T J and Zhou L 2012 *Opt. Lett.* **37** 4940
[10] Huang L L, Chen X Z, Mühlenbernd H, Zhang H, Chen S M, Bai B F, Tan Q F, Jin G F, Cheah K W, Qiu C W, Li J S, Zentgraf T and Zhang S 2013 *Nat. Commun.* **4** 2808
[11] Wen D D, Yue F Y, Li G X, Zheng G X, Chan K L, Chen S M, Chen M, Li K F, Wong P W H, Cheah K W, Pun E Y B, Zhang S and Chen X Z 2015 *Nat. Commun.* **6** 8241
[12] Li J S, Zhao Z J and Yao J Q 2017 *Opt. Express* **25** 29983
[13] Liang L J, Qi M Q, Yang J, Shen X P, Zhai J Q, Xu W Z, Jin B B, Liu W W, Feng Y J, Zhang C H, Lu H, Chen H T, Kang L, Xu W W, Chen J, Cui T J, Wu P H and Liu S G 2015 *Adv. Opt. Mater.* **3** 1374
[14] Zhao J, Cheng Q, Wang T Q, Yuan W and Cui T J 2017 *Opt. Express* **25** 1050
[15] Xu H, Ma S, Ling X, Zhang X, Tang S, Cai T, Sun S, He Q and Zhou L 2018 *ACS Photon.* **5** 1691
[16] Berry M V 1987 *J. Mod. Opt.* **34** 1401
[17] Ding X M, Monticone F, Zhang K, Zhang L, Gao D L, Burokur S N, Lustrac A, Wu Q, Qiu C W and Alù A 2015 *Adv. Mater.* **27** 1195
[18] He X X, Wang G M, Cai T, Xiao J and Zhuang Y Q 2016 *Opt. Express* **24** 27836
[19] Gao L H, Cheng Q, Yang J, Ma S J, Zhao J, Liu S, Chen H B, He Q, Jiang W X, Ma H F, Wen Q Y, Liang L J, Jin B B, Liu W W, Zhou L, Yao J Q, Wu P H and Cui T J 2015 *Light: Sci. & Appl.* **4** e324
[20] Cui T J, Qi M Q, Wan X, Zhao J and Cheng Q 2014 *Light: Sci. &Appl.* **3** e218